# Discriminating Nanoparticle Dimers from Higher Order Aggregates through Wavelength-Dependent SERS Orientational Imaging

**Sarah M. Stranahan, Eric J. Titus, and Katherine A. Willets***

Department of Chemistry and Biochemistry, The University of Texas at Austin, 1 University Station A5300, Austin, Texas 78712, United States.

**ABSTRACT**

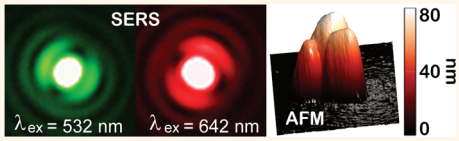


Surface-enhanced Raman scattering (SERS) orientational imaging is a recently developed all-optical technique able to determine SERS-active silver nanoparticle dimer orientations by observing lobe positions in SERS emission patterns formed by the directional polarization of SERS along the longitudinal axis of the dimer. Here we extend this technique to discriminate nanoparticle dimers from higher order aggregates by observing the wavelength dependence of SERS emission patterns, which are unchanged in nanoparticle dimers but show differences in higher order aggregates involving two or more nanoparticle junctions. The ability of SERS orientational imaging to identify stacked nanoparticles in higher order aggregates is also demonstrated. The shape of the SERS emission patterns originating from trimers labeled with low and high concentrations of dye is investigated, showing that the emission pattern lobes become less defined as the dye concentration increases. Dynamic fluctuations in the SERS emission pattern lobes are observed in aggregates labeled with low dye concentrations, as molecules diffuse into regions of higher electromagnetic enhancement in multiple nanoparticle junctions.

**KEYWORDS:** orientational imaging · SERS · nanoparticles · polarization · emission patterns

Over the past two decades, researchers have worked to develop rationally designed surface-enhanced Raman scattering (SERS) substrates to enable the highest possible SERS enhancements.[1−7] In particular, researchers have targeted nanoparticle aggregates (dimers, trimers, *etc.*) due to the formation of "hot spots" or regions of strongly enhanced electromagnetic fields that occur in the junction region between adjacent nanoparticles.[8−12] Correlating the SERS properties and enhancement factor with the corresponding structure of the nanoparticle aggregates is of great importance for developing more well-defined and reproducible SERS substrates.[13−17] Conventionally, this type of correlation study is done by acquiring SERS optical data followed by transferring the sample to an electron microscope to acquire the corresponding nanoparticle structural data. Electron microscopy is not only expensive but also damaging to the sample and cannot be performed at the same time as the SERS data are acquired. However, structural correlation is of high importance in assessing and comparing the SERS enhancement properties of noble metal nanostructures, especially in populations where mixtures of dimers and higher order aggregates may be present.[18−22]

Optical characterization of dimer structure and orientation is most often accomplished by measuring the polarization-dependent localized surface plasmon resonance (LSPR) scattering spectra from assembled or fabricated dimers.[23−29] For these studies, the nanoparticle aggregates are typically analyzed one at a time in order to determine the polarized LSPR response over the full spectral range, reducing the throughput of this approach. Moreover, while this strategy works well for fabricated or homogeneous dimers, challenges arise for heterogeneous systems. Dimer LSPR spectra strongly depend on the orientation, shape, and size of the individual nanoparticles that comprise the dimer, leading to significant differences between individual dimer spectra.[23,24,30] As a result, it is not straightforward to discriminate dimers from higher order aggregates, such as trimers or tetramers, which also show strong variations in their polarization-dependent Rayleigh scattering, depending on the shape and relative orientations of

* Address correspondence to kwillets@mail.utexas.edu.

Received for review December 12, 2011 and accepted January 24, 2012.

**Published online January 24, 2012**
10.1021/nn204866c

the nanoparticles.[31−34] Because of these challenges, polarization-dependent Rayleigh scattering is not always a useful strategy for structural assignment in complex nanoparticle systems and is often accompanied by corresponding structural analysis such as electron microscopy.

In a recent publication, we demonstrated the ability to use optical imaging for determining the alignment of SERS-active silver nanoparticle dimers by analyzing the SERS emission pattern resulting from an excited Rhodamine 6G (R6G) molecule(s) adsorbed to the dimer surface.[35] SERS orientational imaging of a nanoparticle dimer is analogous to single-molecule orientational imaging using defocused fluorescence, but instead of measuring the pattern produced by the spatially directed emission from an emitting dipole, we measure the pattern from polarized SERS emission coupled to and emitted from the longitudinal plasmon mode of a nanoparticle dimer.[36−43] Unlike single-molecule orientational imaging, SERS images do not need to be defocused to observe emission patterns because the inherent high-signal nature of SERS produces enough high-angle light to form the emission pattern features. In this paper, we demonstrate the ability of wavelength-dependent SERS orientational imaging to discriminate between nanoparticle dimers and higher order aggregates, allowing for all-optical structural characterization. Shegai *et al.* have shown that SERS originating from dye-labeled nanoparticle dimers is linearly polarized along the long axis of the dimer, independent of the excitation wavelength, while the polarization properties of SERS from a nanoparticle trimer changes with excitation wavelength.[44] In the dimer case, the linear polarized SERS emission is not excitation wavelength-dependent because it is coupled to a single plasmon mode: the longitudinal plasmon parallel to the long axis of the dimer.[44,45] As a result, we expect the SERS emission pattern, which reflects the polarized emission from the SERS-active dimer, to also be independent of the excitation wavelength. In the case of a trimer, multiple nanoparticle junctions are present, leading to coupling between different plasmon modes. For a molecule coupled to one of the junctions in the trimer, symmetry breaking caused by the presence of the third nanoparticle will lead to a rotation of the emission polarization away from the long axis of the occupied junction. The degree to which the third nanoparticle can perturb the SERS emission properties depends on the excitation wavelength, leading to different emission polarization properties as the excitation wavelength is changed. Because the polarization of SERS originating from a higher order aggregate changes with wavelength, the appearance of the SERS emission pattern will also change with wavelength, serving as an optical signature of a higher order aggregated structure. This technique has several advantages over the polarization-dependent Rayleigh scattering described above: first, it is a high-throughput imaging technique, allowing multiple nanostructures to be analyzed simultaneously, and second, it is insensitive to nanoparticle heterogeneity and is able to discriminate dimers from higher order aggregates regardless of the component nanoparticle shape and size.

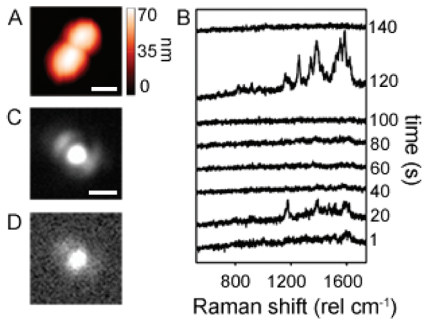


**Figure 1. (A) AFM topography of a SERS-active Nile Blue labeled (∼1 nM) nanoparticle dimer with (B) corresponding selected SERS spectra taken over 140 s with 1 s acquisition times. (C) Nile Blue SERS emission pattern image corresponding to the spectrum taken at 120 s, and (D) background emission image corresponding to the spectrum taken at 100 s. The emission images are acquired with 0.2 s acquisitions. The scale bar in A is 100 nm, and the scale bar in C is 1 $\mu$m.**

## RESULTS AND DISCUSSION

Figure 1 demonstrates correlated spectral and SERS emission pattern imaging for a nanoparticle dimer labeled with Nile Blue (a nonfluorescent analyte). The Nile Blue concentration (∼1 nM) is in the regime typically associated with few- or single-molecule activity, verified by the on/off intensity fluctuations of the SERS spectra in Figure 1B, with the low intensity spectra only showing background signal. Seven hundred SERS images and 140 corresponding spectra are acquired over 140 s, with integration times of 0.2 and 1 s, respectively. Figure 1C shows a SERS emission image from a single image frame, which corresponds to the spectrum acquired at time 120 s. The lobes of the SERS emission pattern lie on either side of the long axis of the nanoparticle dimer as determined by AFM (Figure 1A), allowing for the orientation of the dimer to be determined from the optical emission image alone. Figure 1D shows an emission image from an image frame corresponding to the low-intensity background spectrum taken at time 100 s. Resolved lobes are not apparent in this image; however, when compared with the SERS emission image in 1C, the background emission image shows a similar intensity distribution, with higher intensity on either side of the central feature perpendicular to the long axis of the dimer. This indicates that the background signal is also plasmon-mediated and has some polarization defined by the longitudinal plasmon mode of the dimer. We have chosen to use Nile Blue as our SERS

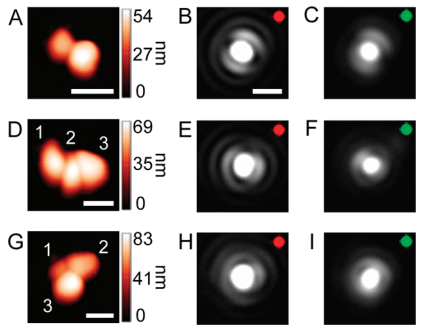


**Figure 2. (A,D,G) AFM topography images of SERS-active silver nanoparticle aggregates, labeled with a low concentration of Nile Blue (1 nM). Correlated Nile Blue SERS emission patterns (B,E,H) excited with 642 nm excitation and (C,F,I) excited with 532 nm excitation, originating from the respective nanostructures. The scale bars in the AFM images all correspond to 100 nm, and the scale bar in the optical image in B is 1 $\mu$m. The colored dots indicate the excitation wavelength color, with a red dot corresponding to 642 nm excitation and a green dot corresponding to 532 nm excitation.**

tag because it has an extremely low fluorescence quantum efficiency in polar solvents such as ethanol and water, which are the only solvents expected to be present on the nanoparticle surface due to the sample preparation and ambient imaging conditions, respectively.[46] Moreover, our SERS spectra do not show any features of Nile Blue fluorescence, as previously reported by Galloway *et al.* on silver nanoparticles.[46] Because of this, we are confident that the background signal is not molecular fluorescence and is therefore most likely silver luminescence from the dimer.[47,48] Recent super-resolution optical studies in our laboratory suggest silver luminescence is plasmon-mediated, and thus we expect it to track with the orientation of the nanoparticle dimer.[49] The low signal and poorly understood mechanism of silver luminescence make it difficult to use luminescence in place of SERS to identify nanoparticle orientations through orientational imaging; however, it may provide useful information in instances where the inclusion of organic dyes is not possible.[47,48]

In the above data, a plate beamsplitter was installed in our optical microscope in order to acquire SERS emission images at the same time as SERS spectra. The inclusion of spectral data is useful in determining the phenomenological origin of the patterns seen in the emission images and verifying that SERS is the responsible mechanism; however, the beamsplitter does not reflect or transmit s- and p-polarized light equally. The polarization of the SERS emission and the orientation and shape of the nanoparticles of interest are intimately connected, and therefore, acquiring SERS emission images through a plate beamsplitter will not give the most accurate information about the nanoparticle orientations. All emission images after Figure 1 are taken with a mirror in place of the beamsplitter, and therefore, no spectral data are taken in parallel. Additionally, quasi-circularly polarized excitation light is used to excite all emission images after Figure 1 to access all plasmon modes in the nanoparticle aggregates of interest.

Varying the SERS excitation wavelength can be used to differentiate nanoparticle dimers from larger aggregates, as described above. In the dimer case, such as the one pictured in Figure 2A, different excitation wavelengths do not change the orientation of the SERS emission pattern lobes in relation to the central feature in Figure 2B,C when excited by a 642 and 532 nm laser, respectively. The emission patterns remain consistent because there is only one plasmon mode coupling to and polarizing the SERS emission. Changing the excitation wavelength will change the measured intensity of the SERS if the plasmon mode is excited more efficiently by one excitation wavelength over the other but will not change the output polarization of the emitted SERS.[44,50] We also note that 642 nm is resonant with the absorption spectrum of Nile Blue, leading to surface-enhanced resonance Raman scattering (SERRS) in this case; however, this does not change the observed emission pattern because the plasmon dictates the polarization of the emission.

In the case of a trimer with two nanoparticle junctions, such as the one pictured in Figure 2D, there are two possible SERS-active junctions: the first along the long axis between particles one and two, and the second along the long axis between particles two and three. Because of the low concentration of Nile Blue used in these studies, we expect that one junction will be occupied, while the other unoccupied, if we are indeed at the single-molecule limit (as indicated by fluctuations in the measured intensity over time). The corresponding SERS emission pattern lobes seen in Figure 2E are not oriented parallel to either of the junctions, in contrast to the dimer example, due to the presence of multiple nanoparticles, which leads to plasmon-mode mixing, as described by Shegai *et al.*[44] Because of the presence of a third nanoparticle, the symmetry of the system is broken, rotating the polarization of the emitted light away from the occupied nanoparticle junction and also generating elliptically polarized, rather than linearly polarized, emission. Using the SERS emission pattern to determine which junction is occupied by the single emitter and therefore responsible for the SERS emission is complex and will be the focus of a future publication but is dependent on many factors including the spacing between the different nanoparticles, the size of the nanoparticles, the position of the nanoparticles relative to each other, and the excitation wavelength.[51] We can, however, utilize the influence of these coupled plasmon modes to discriminate between nanoparticle dimers and higher order aggregates by exciting SERS with two different excitation wavelengths. The ability of the SERS emission to couple to these symmetry-broken

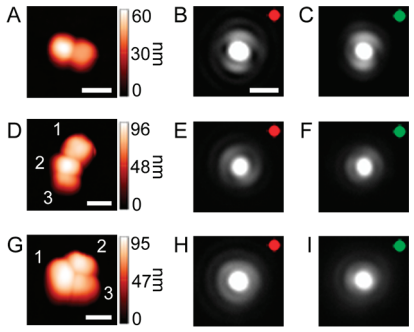


**Figure 3. (A,D,G) AFM topography images of SERS-active silver nanoparticle aggregates, labeled with a high concentration of Nile Blue (100 nM). Correlated Nile Blue SERS emission patterns (B,E,H) excited with 642 nm excitation and (C,F,I) excited with 532 nm excitation originating from the respective nanostructures. The scale bars in the AFM images all correspond to 100 nm, and the scale bar in the optical image in B is 1 $\mu$m.**

plasmon modes will be wavelength-dependent, and therefore, the lobes of the SERS emission patterns originating from nonlinear trimers will not be identical at two different excitation wavelengths. This excitation wavelength dependence is apparent in the SERS emission patterns originating from the trimer in Figure 2D excited by 642 nm (Figure 2E) and 532 nm (Figure 2F). The axis perpendicular to the emission pattern lobes rotates by approximately 15° between 2E and 2F, due to the wavelength-dependent rotation of the polarized emission.

The trimer in Figure 2G has three nanoparticle junctions and, therefore, has three possible SERS-active sites. As with the trimer in Figure 2D, the lobes of the SERS emission patterns in Figure 2H and Figure 2I rotate as the excitation wavelength is changed from 642 to 532 nm, respectively. Unlike the previous examples, the emission pattern lobes are less defined in both of these images, indicating that the emitted light is most likely more strongly elliptically polarized, especially in comparison to the dimer example. The higher image contrast in the 642 nm excited Nile Blue SERS emission patterns may stem from the resonance of the first electronic transition of Nile Blue with 642 nm excitation, producing a higher overall signal-to-noise. Also, longer wavelengths are not focused as tightly as shorter wavelengths, spreading the emission pattern images from 642 nm excited SERS emission patterns over more camera pixels compared to the 532 nm excited SERS emission patterns. Because of the fluctuating signal intensity and low signal-to-noise in some cases, the SERS emission patterns in Figures 2–5 are the sum of several high-intensity image frames, recontrasted in the imaging software to make the emission pattern lobes easier to see.

The nanoparticles in Figure 2 clearly demonstrate that excitation wavelength-dependent SERS orientational imaging allows dimers and higher order aggregates to be discriminated in the single- or few-molecule

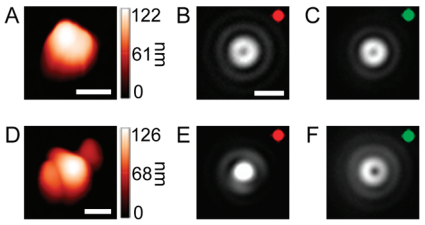


**Figure 4. (A) AFM topography of a SERS-active silver nanoparticle stacked dimer and (B,C) the corresponding SERS emission pattern images excited with (B) 642 nm and (C) 532 nm light. (D) AFM topography of a higher order nanoparticle aggregate containing a strong out-of-plane plasmon mode. (E,F) Corresponding SERS emission pattern images excited with (E) 642 nm and (F) 532 nm light. The scale bars in A and D are 100 nm, and the scale bar in B is 1 $\mu$m.**

labeling regime. In Figure 3, we investigate how dye labeling concentration affects the appearance of the SERS emission patterns. For these examples, the Nile Blue concentration is increased 2 orders of magnitude, to ~100 nM, allowing for multiple junctions to be occupied in the case of higher order aggregates. For the dimer pictured in Figure 3A–C, the SERS emission pattern lobes remain resolved from the central feature and appear similar to those in the low concentration labeled dimer in Figure 2. This discrete nature of the SERS emission pattern lobes at high dye concentrations reconfirms that the longitudinal plasmon mode of the dimer dominates the SERS emission polarization, producing linear polarized emission oriented along the long axis of the nanoparticle dimer. The position of the SERS emission pattern lobes of the dimer in Figure 3B,C are wavelength-independent when excited by 642 and 532 nm excitation, respectively.

The position of the SERS emission pattern lobes originating from the two-junction trimer in Figure 3D remains wavelength-dependent, even at higher dye concentrations, with the 642 nm excited SERS emission pattern lobes in Figure 3E rotated approximately 45° from the 532 nm excited SERS emission pattern lobes in Figure 3F. The positions of the lobes in the 642 nm excited SERS emission pattern in 3E appear to be influenced more by the longitudinal plasmon mode between particles 1 and 2, while the lobes in the 532 nm excited SERS emission pattern in 3F appear more strongly influenced by the longitudinal plasmon mode between particles 2 and 3. This is most likely due to stronger excitation of one plasmon mode at a particular wavelength, due to the difference in size between the nanoparticles. Despite the high density of dye on the nanoparticle surface, we still observe a strong wavelength dependence in the SERS emission from this asymmetric trimer.

Figure 3G shows a more symmetric trimer with three junctions that are all expected to be SERS-active. Previous work from Käll has shown that trimer structures with a high degree of symmetry show nearly

isotropic emission polarization behavior.[50] The SERS emission pattern excited by 642 nm (Figure 3H) appears like a nearly symmetric ring around the bright central feature, consistent with isotropic emission. The 532 nm excited SERS emission pattern in Figure 3I shows a similar ring pattern around the central feature, although with a slight bias toward the upper left, providing a small, but distinct, difference in the two emission patterns. The smearing of the lobe features in the emission patterns in 3H and 3I into an isotropic ring pattern results from SERS originating from a higher number of molecules present in multiple junctions, creating an overall SERS signal with a more isotropic polarization. This type of ring emission is not possible in a nanoparticle dimer, providing us with an easily identifiable characteristic of the presence of a higher order aggregate. Moreover, when screening nanoparticles labeled with high concentrations of dye, this strategy allows simple discrimination of dimers, asymmetrically assembled trimers, and symmetrically assembled trimers for rapid comparison of SERS signal enhancements as a function of available SERS-active junctions. We have repeated this experiment using an even higher dye labeling concentration (10 $\mu$M) and observed identical results. We note that as the cluster sizes increase beyond trimers and possibly tetramers, our ability to identify structures diminishes, although we are still able to uniquely discriminate dimers from other higher order structures.

If we return to the low dye concentration (1 nM Nile Blue) samples, we look at nanoparticle aggregates possessing plasmon modes oriented vertically to the sample plane.[35] The simplest case of a vertically oriented plasmon mode is one nanoparticle stacked directly on top of a second nanoparticle, which is the case with the nanoparticle dimer in Figure 4A. The only clue in the AFM topography image in Figure 4A that we have two stacked nanoparticles is that the height of the nanostructure is 122 nm, which is higher than the average single nanoparticle (usually between 50 and 90 nm in height). However, the radially symmetric donut shape of the SERS emission patterns in Figure 4B,C reveals the presence of the vertically oriented plasmon mode.[36,52] The SERS emission patterns excited by the 642 and 532 nm lasers in Figure 4B, C appear identical because there must be only one longitudinal plasmon mode present to couple with the SERS, as described previously for the in-plane nanoparticle dimers. Thus, despite the lack of structural information provided by AFM, we are confident that the nanoparticle in Figure 4A is a stacked nanoparticle dimer, based on orientational imaging.

The nanoparticle aggregate example in Figure 4D, on the other hand, is composed of at least four nanoparticles. The lobes and solid central feature of the 642 nm excited SERS emission pattern in Figure 4E indicate that the emission originates from a plasmon mode located in the plane of the sample. However, the asymmetric donut shape of the 532 nm excited SERS emission pattern in Figure 4F reveals the presence of an out-of-plane plasmon mode that is strongly coupled to the higher energy excitation. As with the previous examples, we observe a change in the wavelength-dependent emission pattern for the higher order aggregate, which is not observed for the vertically stacked dimer in Figure 4A. These data further confirm our ability to use SERS orientational imaging to assign the structure of SERS-active nanoparticles, even when traditional structural imaging strategies such as AFM fail to provide sufficient topographical information.

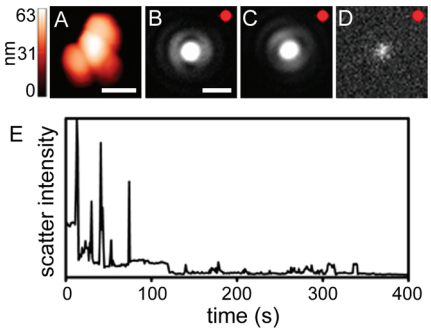


**Figure 5. (A) AFM topography of a SERS-active silver nanoparticle tetramer labeled with a low concentration of Nile Blue (1nM). Correlated Nile Blue SERS emission patterns excited by 642 nm excitation acquired during (B) time = 0–1 s and (C) time = 76–115 s. (D) Luminescent background emission pattern acquired during time = 396 s. (E) Integrated SERS intensity *vs* time plot showing the time-dependent fluctuation in the Nile Blue SERS. The scale bar in A is 100 nm, and the scale bar in B is 1 $\mu$m.**

Again considering the low dye concentration (1 nM Nile Blue) samples, we note that we occasionally observe dynamic switching of the SERS emission pattern lobes between two different orientations. Figure 5 shows an example of a nanoparticle tetramer (Figure 5A) that displays this switching behavior. The integrated Nile Blue SERS intensity excited by a 642 nm laser is plotted as a function of time over 400 s in Figure 5E. The SERS intensity fluctuates with time, indicative of single- or few-molecule SERS. The SERS emission pattern images taken during the first second of the acquisition are added together to produce the image in Figure 5B and show polarized emission oriented in the vertical direction. Figure 5C shows the SERS emission pattern from the same nanoparticle excited by 642 nm, corresponding to the sum of 40 image frames acquired between 76 and 115 s. During this later time, the SERS emission pattern has rotated from the original orientation to a new orientation, offset by nearly 70°. Previous calculations from Xu and co-workers have shown that the emission polarization from a molecule located in a fixed nanoparticle junction is stable, regardless of the orientation of the molecule.[51] Thus, the discrete switching behavior of

the SERS emission patterns indicates that the SERS emission is originating from a different junction within the tetramer. This is excellent evidence that we are observing single- or few-molecule SERS from molecules that are dynamically exploring the nanoparticle surface, consistent with our previous work using super-resolution imaging.[17,49] For comparison, Figure 5D shows the background emission from the silver nanoparticle aggregate at time 396 s when no SERS is present and only luminescence is expected. No distinct emission pattern features are apparent in the background emission image because the signal is very low due to the poor excitation of silver luminescence at 642 nm.[53,54] This verifies that the signal in Figure 5B,C is originating from a SERS-active molecule, exploring spatially distinct junctions on the surface of the nanoparticle tetramer.

## CONCLUSIONS

In conclusion, we have extended the application of SERS orientational imaging to discriminate between silver nanoparticle dimers and higher order aggregates including stacked aggregates by imaging SERS emission patterns at two different excitation wavelengths and observing changes in the SERS emission patterns. We demonstrated that this strategy works at both high and low dye labeling concentrations and discussed how different dye concentrations affect the appearance of the emission patterns in dimers *versus* trimers with two or three SERS active junctions. The SERS emission patterns from nanoparticle dimers were unaffected by both excitation wavelength and dye labeling concentration, unlike the lobes of the two-junction and three-junction trimer SERS emission patterns that change with excitation wavelength and appeared more elliptically or even circularly polarized at the higher dye labeling concentration. A benefit to working at a low dye labeling concentration is the possibility of observing dynamic changes in the SERS emission patterns as molecules probe multiple nanoparticle junction regions. Our next step is to develop a model to describe wavelength-dependent SERS emission patterns in higher order aggregates. This goal will move us closer to an all-optical far-field imaging technique able to describe nanoparticle structure and map SERS-active plasmon modes in higher order nanoparticle aggregates. However, even without a model, SERS orientational imaging provides a rapid, all-optical technique for structural discrimination of nanoparticle dimers from higher order aggregates, which is critical for characterizing rationally designed SERS substrates.

## METHODS

**SERS Sample Preparation.** SERS samples with a final Nile Blue concentration of ~1 nM are made by adding 10 $\mu$L of ~21 nM Nile Blue in ethanol to 100 $\mu$L of silver colloid aggregates in nanopure water prepared by the Lee and Meisel method.[55] The sample is vortexed for 30 s, and then 100 $\mu$L of 20 mM NaBr in water is added, followed by vortexing for 30 s. The NaBr solution is added to induce nanoparticle aggregations. SERS samples with a final Nile Blue concentration of ~100 nM are made in the same manner with a ~2.1 $\mu$M Nile Blue solution. Piranha-cleaned glass slides are patterned with an alpha-numeric aluminum grid by shadow deposition of 40 nm of aluminum through TEM grids taped to glass slides. It should be noted that working with Piranha solution is extremely dangerous. A patterned glass slide is then submerged in a 2% APTES methanol solution for up to 5 min followed by copious rinsing with methanol to remove excess APTES and then rinsed by nanopure water and dried under nitrogen. One microliter of the SERS solution is drop-cast onto the center of the APTES-coated patterned glass slide and is allowed to sit for a few seconds before being blown off with streaming nitrogen. The slide is then rinsed copiously with nanopure water to remove excess salt and dried under nitrogen again. The APTES immobilizes the nanoparticles on the glass slide to optimize nanoparticle coverage and to decrease the possibility of being moved during AFM imaging.

**Optical Experiments.** Optical experiments are carried out on an Olympus IX-71 inverted microscope with an Olympus UPlanFLN 100× oil immersion objective with a 1.30 numerical aperture. Nile Blue SERS is excited either by a 208 W/cm$^2$ 642 nm laser or a 422 W/cm$^2$ 532 nm laser in epi-illumination, and the resulting scatter is imaged onto a Princeton Instruments ProEM 512 electron-multiplied charge-coupled device (EM-CCD) camera. The excitation lasers are passed through a quarter wave plate to produce quasi-circularly polarized light with a 68:32 max/min polarization ratio for the 642 nm laser and a 59:41 max/min polarization ratio for the 532 nm laser. Dark-field scattering images of the same region of interest are also collected using a dark-field condenser in transmission geometry. The optical data in Figure 1 of this article are taken in the same manner with the addition of a 50/50 beamsplitter sending half of the collected scatter to a Princeton Instruments ACTON SpectraPro 2500i spectrograph with a 1200 g/mm grating onto a Spec-10 liquid nitrogen cooled CCD camera.

**AFM Correlation.** Following SERS emission pattern imaging with the EM-CCD optical setup, the sample slide is moved to a combined inverted optical microscope (Olympus IX-71) and AFM (NT-MDT NTEGRA Vita) setup. Bright-field images are collected with the AFM optical viewing system, while dark-field images are collected *via* white light through-the objective total internal reflection (TIR) using a 60× Olympus total internal reflection fluorescence (TIRF) oil immersion objective with a 1.45 numerical aperture. All AFM scans are collected in tapping mode using NT-MDT NSG30 semicontact silicon probes. This system has been described in detail in ref 23.

*Conflict of Interest:* The authors declare no competing financial interest.

*Acknowledgment.* S.M.S. gratefully acknowledges the NSF IGERT "Atomic and Molecular Imaging" Program (Grant No. DGE-0549417) for fellowship support. We also thank the Welch Foundation in support of the facilities utilized in the Center for Nano and Molecular Science at the University of Texas at Austin. This material is based upon work supported by the Welch Foundation under Award No. F-1699 and the Air Force Office of Scientific Research under AFOSR Award No. FA9550-09-0122.

*Supporting Information Available:* AFM images of additional nanoparticle dimer/aggregate examples, associated SERS emission patterns and LSPR spectra. This material is available free of charge *via* the Internet at http://pubs.acs.org.

## REFERENCES AND NOTES


1. Schwartzberg, A. M.; Oshiro, T. Y.; Zhang, J. Z.; Huser, T.; Talley, C. E. Improving Nanoprobes Using Surface-Enhanced Raman Scattering from 30-nm Hollow Gold Particles. *Anal. Chem.* **2006**, *78*, 4732–4736.
2. Stiles, P. L.; Dieringer, J. A.; Shah, N. C.; Van Duyne, R. P. Surface-Enhanced Raman Spectroscopy. *Annu. Rev. Anal. Chem.* **2008**, *1*, 601–626.
3. Jaeckel, F.; Kinkhabwala, A. A.; Moerner, W. E. Gold Bowtie Nanoantennas for Surface-Enhanced Raman Scattering under Controlled Electrochemical Potential. *Chem. Phys. Lett.* **2007**, *446*, 339–343.
4. Banholzer, M. J.; Millstone, J. E.; Qin, L.; Mirkin, C. A. Rationally Designed Nanostructures for Surface-Enhanced Raman Spectroscopy. *Chem. Soc. Rev.* **2008**, *37*, 885–897.
5. Michaels, A. M.; Nirmal, M.; Brus, L. E. Surface Enhanced Raman Spectroscopy of Individual Rhodamine 6G Molecules on Large Ag Nanocrystals. *J. Am. Chem. Soc.* **1999**, *121*, 9932–9939.
6. Van Duyne, R. P.; Hulteen, J. C.; Treichel, D. A. Atomic Force Microscopy and Surface-Enhanced Raman Spectroscopy. I. Silver Island Films and Silver Film over Polymer Nanosphere Surfaces Supported on Glass. *J. Chem. Phys.* **1993**, *99*, 2101–2115.
7. Talley, C. E.; Jackson, J. B.; Oubre, C.; Grady, N. K.; Hollars, C. W.; Lane, S. M.; Huser, T. R.; Nordlander, P.; Halas, N. J. Surface-Enhanced Raman Scattering from Individual Au Nanoparticles and Nanoparticle Dimer Substrates. *Nano Lett.* **2005**, *5*, 1569–1574.
8. Futamata, M.; Maruyama, Y.; Ishikawa, M. Critical Importance of the Junction in Touching Ag Particles for Single Molecule Sensitivity in SERS. *J. Mol. Struct.* **2005**, *735*−*736*, 75–84.
9. Hao, E.; Schatz, G. C. Electromagnetic Fields around Silver Nanoparticles and Dimers. *J. Chem. Phys.* **2004**, *120*, 357–366.
10. Haran, G. Single-Molecule Raman Spectroscopy: A Probe of Surface Dynamics and Plasmonic Fields. *Acc. Chem. Res.* **2010**, *43*, 1135–1143.
11. Jiang, J.; Bosnick, K.; Maillard, M.; Brus, L. Single Molecule Raman Spectroscopy at the Junctions of Large Ag Nanocrystals. *J. Phys. Chem. B* **2003**, *107*, 9964–9972.
12. Schatz, G. C.; Young, M. A.; Van Duyne, R. P. Electromagnetic Mechanism of SERS. *Top. Appl. Phys.* **2006**, *103*, 19–46.
13. Camden, J. P.; Dieringer, J. A.; Wang, T.; Masiello, D. J.; Marks, L. D.; Schatz, G. C.; Van Duyne, R. P. Probing the Structure of Single-Molecule Surface-Enhanced Raman Scattering Hot Spots. *J. Am. Chem. Soc.* **2008**, *130*, 12616–12617.
14. Kaplan-Ashiri, I.; Titus, E. J.; Willets, K. A. Subdiffraction-Limited Far-Field Raman Spectroscopy of Single Carbon Nanotubes: An Unenhanced Approach. *ACS Nano* **2011**, *5*, 1033–1041.
15. Kumar, R.; Zhou, H.; Cronin, S. B. Surface-Enhanced Raman Spectroscopy and Correlated Scanning Electron Microscopy of Individual Carbon Nanotubes. *Appl. Phys. Lett.* **2007**, *91*, 223105/223101–223105/223103.
16. Rycenga, M.; Camargo, P. H. C.; Li, W.; Moran, C. H.; Xia, Y. Understanding the SERS Effects of Single Silver Nanoparticles and Their Dimers, One at a Time. *J. Phys. Chem. Lett.* **2010**, *1*, 696–703.
17. Weber, M. L.; Willets, K. A. Correlated Super-Resolution Optical and Structural Studies of Surface-Enhanced Raman Scattering Hot Spots in Silver Colloid Aggregates. *J. Phys. Chem. Lett.* **2011**, *2*, 1766–1770.
18. Nie, S.; Emory, S. R. Probing Single Molecules and Single Nanoparticles by Surface-Enhanced Raman Scattering. *Science* **1997**, *275*, 1102–1106.
19. Michaels, A. M.; Jiang, J.; Brus, L. Ag Nanocrystal Junctions as the Site for Surface-Enhanced Raman Scattering of Single Rhodamine 6G Molecules. *J. Phys. Chem. B* **2000**, *104*, 11965–11971.
20. van Dijk, M. A.; Lippitz, M.; Orrit, M. Far-Field Optical Microscopy of Single Metal Nanoparticles. *Acc. Chem. Res.* **2005**, *38*, 594–601.
21. Chen, G.; Wang, Y.; Yang, M.; Xu, J.; Goh, S. J.; Pan, M.; Chen, H. Measuring Ensemble-Averaged Surface-Enhanced Raman Scattering in the Hotspots of Colloidal Nanoparticle Dimers and Trimers. *J. Am. Chem. Soc.* **2010**, *132*, 3644–3645.
22. Wustholz, K. L.; Henry, A.-I.; McMahon, J. M.; Freeman, R. G.; Valley, N.; Piotti, M. E.; Natan, M. J.; Schatz, G. C.; Van Duyne, R. P. Structure−Activity Relationships in Gold Nanoparticle Dimers and Trimers for Surface-Enhanced Raman Spectroscopy. *J. Am. Chem. Soc.* **2010**, *132*, 10903–10910.
23. Brown, L. V.; Sobhani, H.; Lassiter, J. B.; Nordlander, P.; Halas, N. J. Heterodimers: Plasmonic Properties of Mismatched Nanoparticle Pairs. *ACS Nano* **2010**, *4*, 819–832.
24. Grillet, N.; Manchon, D.; Bertorelle, F.; Bonnet, C.; Broyer, M.; Cottancin, E.; Lerme, J.; Hillenkamp, M.; Pellarin, M. Plasmon Coupling in Silver Nanocube Dimers: Resonance Splitting Induced by Edge Rounding. *ACS Nano* **2011**, *5*, 9450–9462.
25. Jain, P. K.; El-Sayed, M. A. Plasmonic Coupling in Noble Metal Nanostructures. *Chem. Phys. Lett.* **2010**, *487*, 153–164.
26. Rechberger, W.; Hohenau, A.; Leitner, A.; Krenn, J. R.; Lamprecht, B.; Aussenegg, F. R. Optical Properties of Two Interacting Gold Nanoparticles. *Opt. Commun.* **2003**, *220*, 137–141.
27. Rong, G.; Wang, H.; Reinhard, B. M. Insights from a Nanoparticle Minuet: Two-Dimensional Membrane Profiling through Silver Plasmon Ruler Tracking. *Nano Lett.* **2010**, *10*, 230–238.
28. Sheikholeslami, S.; Jun, Y.-w.; Jain, P. K.; Alivisatos, A. P. Coupling of Optical Resonances in a Compositionally Asymmetric Plasmonic Nanoparticle Dimer. *Nano Lett.* **2010**, *10*, 2655–2660.
29. Wang, H.; Reinhard, B. M. Monitoring Simultaneous Distance and Orientation Changes in Discrete Dimers of DNA Linked Gold Nanoparticles. *J. Phys. Chem. C* **2009**, *113*, 11215–11222.
30. Tabor, C.; Van, H. D.; El-Sayed, M. A. Effect of Orientation on Plasmonic Coupling between Gold Nanorods. *ACS Nano* **2009**, *3*, 3670–3678.
31. Chen, H.; Sun, Z.; Ni, W.; Woo, K. C.; Lin, H.-Q.; Sun, L.; Yan, C.; Wang, J. Plasmon Coupling in Clusters Composed of 2-Dimensionally Ordered Gold Nanocubes. *Small* **2009**, *5*, 2111–2119.
32. Funston, A. M.; Davis, T. J.; Novo, C.; Mulvaney, P. Coupling Modes of Gold Trimer Superstructures. *Philos. Trans. R. Soc., A* **2011**, *369*, 3472–3482.
33. Chuntonov, L.; Haran, G. Effect of Symmetry Breaking on the Mode Structure of Trimeric Plasmonic Molecules. *J. Phys. Chem. C* **2011**, *115*, 19488–19495.
34. Chuntonov, L.; Haran, G. Trimeric Plasmonic Molecules: The Role of Symmetry. *Nano Lett.* **2011**, *11*, 2440–2445.
35. Stranahan, S. M.; Titus, E. J.; Willets, K. A. SERS Orientational Imaging of Silver Nanoparticle Dimers. *J. Phys. Chem. Lett.* **2011**, *2*, 2711–2715.
36. Bartko, A. P.; Dickson, R. M. Imaging Three-Dimensional Single Molecule Orientations. *J. Phys. Chem. B* **1999**, *103*, 11237–11241.
37. Bohmer, M.; Enderlein, J. Orientation Imaging of Single Molecules by Wide-Field Epifluorescence Microscopy. *J. Opt. Soc. Am. B* **2003**, *20*, 554–559.
38. Forkey, J. N.; Quinlan, M. E.; Alexander, S. M.; Corrie, J. E. T.; Goldman, Y. E. Three-Dimensional Structural Dynamics of Myosin V by Single-Molecule Fluorescence Polarization. *Nature* **2003**, *422*, 399–404.
39. Lieb, M. A.; Zavislan, J. M.; Novotny, L. Single-Molecule Orientations Determined by Direct Emission Pattern Imaging. *J. Opt. Soc. Am. B* **2004**, *21*, 1210–1215.
40. Sick, B.; Hecht, B.; Novotny, L. Orientational Imaging of Single Molecules by Annular Illumination. *Phys. Rev. Lett.* **2000**, *85*, 4482–4485.
41. Weiss, S. Measuring Conformational Dynamics of Biomolecules by Single Molecule Fluorescence Spectroscopy. *Nat. Struct. Biol.* **2000**, *7*, 724–729.
42. Etchegoin, P. G.; Galloway, C.; Le, R. E. C. Polarization-Dependent Effects in Surface-Enhanced Raman Scattering (SERS). *Phys. Chem. Chem. Phys.* **2006**, *8*, 2624–2628.

43. Zou, S.; Schatz, G. C. Coupled Plasmonic Plasmon/Photonic Resonance Effects in SERS. *Top. Appl. Phys.* **2006**, *103*, 67–86.
44. Shegai, T.; Li, Z.; Dadosh, T.; Zhang, Z.; Xu, H.; Haran, G. Managing Light Polarization *via* Plasmon–Molecule Interactions within an Asymmetric Metal Nanoparticle Trimer. *Proc. Natl. Acad. Sci. U.S.A.* **2008**, *105*, 16448–16453.
45. Itoh, T.; Biju, V.; Ishikawa, M.; Kikkawa, Y.; Hashimoto, K.; Ikehata, A.; Ozaki, Y. Surface-Enhanced Resonance Raman Scattering and Background Light Emission Coupled with Plasmon of Single Ag Nanoaggregates. *J. Chem. Phys.* **2006**, *124*, 134708/134701–134708/134706.
46. Galloway, C. M.; Etchegoin, P. G.; Le, R. E. C. Ultrafast Nonradiative Decay Rates on Metallic Surfaces by Comparing Surface-Enhanced Raman and Fluorescence Signals of Single Molecules. *Phys. Rev. Lett.* **2009**, *103*, 063003.
47. Itoh, T.; Kikkawa, Y.; Biju, V.; Ishikawa, M.; Ikehata, A.; Ozaki, Y. Variations in Steady-State and Time-Resolved Background Luminescence from Surface-Enhanced Resonance Raman Scattering-Active Single Ag Nanoaggregates. *J. Phys. Chem. B* **2006**, *110*, 21536–21544.
48. Zhang, A.; Zhang, J.; Fang, Y. Photoluminescence from Colloidal Silver Nanoparticles. *J. Lumin.* **2008**, *128*, 1635–1640.
49. Stranahan, S. M.; Willets, K. A. Super-Resolution Optical Imaging of Single-Molecule SERS Hot Spots. *Nano Lett.* **2010**, *10*, 3777–3784.
50. Shegai, T.; Brian, B.; Miljkovic, V. D.; Kall, M. Angular Distribution of Surface-Enhanced Raman Scattering from Individual Au Nanoparticle Aggregates. *ACS Nano* **2011**, *5*, 2036–2041.
51. Li, Z.; Shegai, T.; Haran, G.; Xu, H. Multiple-Particle Nanoantennas for Enormous Enhancement and Polarization Control of Light Emission. *ACS Nano* **2009**, *3*, 637–642.
52. Sick, B.; Hecht, B.; Wild, U. P.; Novotny, L. Probing Confined Fields with Single Molecules and Vice Versa. *J. Microsc.* **2001**, *202*, 365–373.
53. Borys, N. J.; Lupton, J. M. Surface-Enhanced Light Emission from Single Hot Spots in Tollens Reaction Silver Nanoparticle Films: Linear *versus* Nonlinear Optical Excitation. *J. Phys. Chem. C* **2011**, *115*, 13645–13659.
54. Geddes, C. D.; Parfenov, A.; Gryczynski, I.; Lakowicz, J. R. Luminescent Blinking from Silver Nanostructures. *J. Phys. Chem. B* **2003**, *107*, 9989–9993.
55. Lee, P. C.; Meisel, D. Adsorption and Surface-Enhanced Raman of Dyes on Silver and Gold Sols. *J. Phys. Chem.* **1982**, *86*, 3391–3395.